Stochastic Analysis of Electrostatic MEMS Subjected to Parameter Variations

Nitin Agarwal and Narayana R. Aluru

Abstract—**This paper presents an efficient stochastic framework for quantifying the effect of stochastic variations in various design parameters such as material properties, geometrical features, and/or operating conditions on the performance of electrostatic microelectromechanical systems (MEMS) devices. The stochastic framework treats uncertainty as a separate dimension, in addition to space and time, and seeks to approximate the stochastic dependent variables using sparse grid interpolation in the multidimensional random space. This approach can be effectively used to compute important information, such as moments (mean and variance), failure probabilities, and sensitivities with respect to design variables, regarding relevant quantities of interest. The approach is straightforward to implement and, depending on the accuracy required, can be orders of magnitude faster than the traditional Monte Carlo method. We consider two examples—MEMS switch and resonator—and employ the proposed approach to study the effect of uncertain Young's modulus and various geometrical parameters, such as dimensions of electrodes and gap between microstructures, on relevant quantities of interest such as actuation behavior, resonant frequency, and quality factor. It is demonstrated that, in addition to computing the required statistics and probability density function, the proposed approach effectively identifies critical design parameters, which can then be controlled during fabrication, in order to improve device performance and reliability. [2009-0065]**

Index Terms—**Microelectromechanical systems (MEMS) resonator, MEMS switch, parameter variation, reliability, Smolyak algorithm, sparse grid interpolation, uncertainty propagation.**

I. Introduction

MICROELECTROMECHANICAL systems (MEMS) have been used in widespread sensing and actuation applications such as microswitches, gyroscopes, accelerometers, etc. While the potential of such devices is widely recognized, rapid and reliable design of these devices is still a challenging issue. For rapid computational prototyping of such devices, it is required to accurately model the interaction of various physical fields such as mechanical, electrical, and fluidic. In recent years, advances in numerical simulation methods and better understanding of the underlying multiphysics have increased the ability to accurately model these devices [1]–[4]. These simulation methods, however, assume that the geometrical and physical properties of the device are known in a deterministic sense. In reality, significant uncertainties in these properties are unavoidable due to a variety of factors such as low-cost manufacturing processes, residual stresses, irregular surface topography, chemical contamination, etc. [5]. For example, there could always be some uncertainty associated with the geometrical features such as dimensions of the electrodes or gap between two electrodes or the material properties such as the Young's modulus, etc. As a result, development of theoretical and computational models based on pedagogical deterministic approaches can be inaccurate. Therefore, it is imperative that the stochastic variations in various design parameters be considered during the development of computational models.

In the past, MEMS uncertainties have been taken into account through subjective safety factors, which may lead to over conservative designs. Several researchers have used Monte Carlo (MC) simulations to consider the uncertainty associated with various input parameters during the design of electrostatic MEMS. Reh *et al.* [6] studied the effect of various geometrical features on the design of a comb drive using ANSYS probabilistic design system. The variability in the performance of a ceramic MEMS actuator resulting from variations in the shape of the actuator and the air gap in the condenser has been studied in [7]. Recently, several approaches have been proposed for reliability-based design optimization of MEMS devices under uncertainties. Allen *et al.* [8] employed the first-order reliability method for optimizing the tuning accuracy of an electrostatically actuated variable capacitor under reliability constraints. Han and Kwak [9] presented the use of robust optimization during the design of a microgyroscope using MC simulations to compare predicted yields. Liu *et al.* [10] presented a robust design method to minimize the sensitivity of a laterally vibrating resonator against width variations due to fabrication errors. A genetic algorithm based on MC simulations has been used in [5] for optimizing the filter performance of a MEMS resonator in terms of the shape of the frequency-response curve. Wittwer *et al.* [11] applied a robust optimization framework based on Taylor series expansion to design a fully compliant bistable micromechanism under various uncertainties. Most of these optimization frameworks are based on MC simulations, which presents a natural but expensive approach for including uncertainties. Specially, when these uncertainties are considered using high-fidelity computational models for the complex multiphysics MEMS problems, it often becomes impractical due to prohibitive computational cost. In [12] and [13], we

Manuscript received March 18, 2009; revised July 20, 2009. First published November 18, 2009; current version published December 1, 2009. This work was supported in part by the National Science Foundation under Grant 0601479, in part by the Defense Advanced Research Projects Agency/Microsystems Technology Office, and in part by the Department of Energy. Subject Editor D. Elata.

The authors are with the Department of Mechanical Science and Engineering and the Beckman Institute for Advanced Science and Technology, University of Illinois at Urbana–Champaign, Urbana, IL 61801 USA (e-mail: aluru@illinois.edu).

Color versions of one or more of the figures in this paper are available online at http://ieeexplore.ieee.org.

Digital Object Identifier 10.1109/JMEMS.2009.2034612

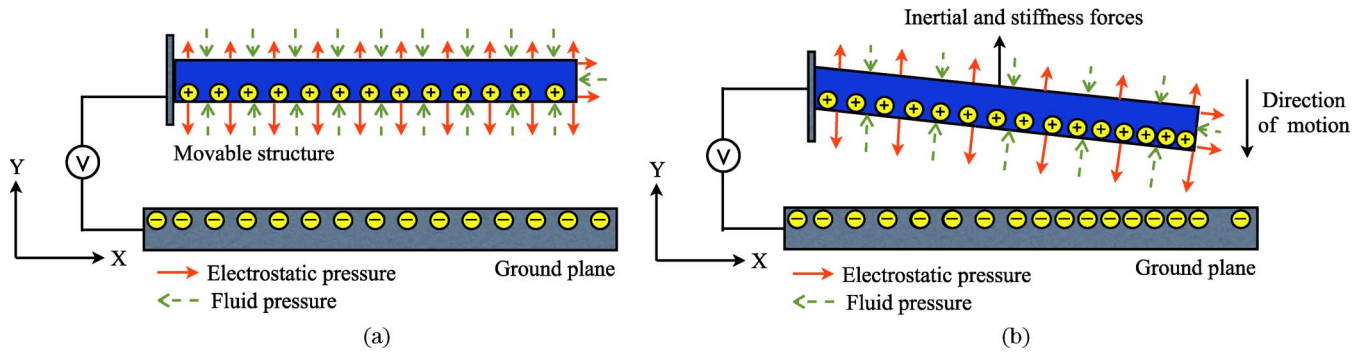

Fig. 1. Illustration of coupling among various energy domains for electrostatic MEMS. (a) Applied voltage gives rise to electrostatic pressure on the beam which is also subjected to ambient fluid (air) pressure at $t = 0$. (b) Deformed structure with various forces acting on it at $t > 0$ (note that the figure does not represent the correct curvature of the beam upon deformation).

presented a stochastic Lagrangian framework for MEMS based on a spectral discretization technique—*generalized polynomial chaos* (GPC)— followed by Galerkin projections, which provides high accuracy and fast convergence. However, the stochastic Galerkin framework leads to a set of coupled deterministic equations that need to be solved, and hence, the implementation may be nontrivial (see [13] for details).

In this paper, we develop a stochastic modeling framework with a twofold objective. The first objective is to quantify the effect of stochastic variations in various design parameters such as material properties, geometrical features, and/or operating conditions on the performance of electrostatic MEMS devices. This involves estimating the statistics such as mean and variance, probability density function (pdf), and sensitivities of relevant quantities of interest corresponding to a given variation in the design variables. The second objective is to employ uncertainty quantification data to identify critical design parameters, which can then be controlled during fabrication, in order to achieve the desired performance.

The proposed stochastic framework treats uncertainty as a separate dimension in addition to physical dimensions (space and time), using which all dependent uncertain parameters are represented as high-dimensional functions. These functions then need to be approximated or *discretized* in both stochastic and physical domains. The stochastic discretization is done using *stochastic collocation (SC) approach* [14]–[16], which seeks to approximate the stochastic dependent variables by constructing interpolants in the multidimensional random space. The interpolation is constructed by sampling the dependent variables at a predetermined set of points, chosen as the sparse grid nodes generated using the Smolyak algorithm [17]. The physical discretization can be performed using finite element method (FEM) and boundary element method (BEM) with appropriate time integration, or any other suitable method of choice. Since this approach only involves sampling at a predetermined set of nodes (like the MC method), it is straightforward to implement and only requires repeated calls to the already existing validated deterministic code for MEMS. Thus, the stochastic implementation is developed as a *wrapper* around the deterministic code. Moreover, for the number of uncertain parameters, one usually needs to consider for the analysis of MEMS devices; this approach is orders of magnitude faster than the MC method to obtain the same level of accuracy. This allows us to consider the effect of uncertainties using high-fidelity computational models, without incurring prohibitive computational cost. We consider two examples—MEMS switch and resonator—and employ the proposed approach to study the effect of uncertain Young's modulus and various geometrical parameters, such as dimensions and gaps between microstructures, on relevant quantities of interest such as actuation behavior, resonant frequency, and quality factor. It is demonstrated that, in addition to computing the required statistics and pdf, the proposed methodology effectively identifies critical design parameters.

The remainder of this paper is organized as follows. In Section II, we present the deterministic and stochastic formulation for the coupled electromechanical problem, applicable to dynamic analysis of electrostatic MEMS. In Section III, we present the SC framework based on sparse grid interpolation for stochastic analysis of MEMS. In Section IV, we demonstrate the proposed methodology by considering several MEMS devices subjected to variations in design parameters. Finally, we conclude the discussion in Section V.

II. Theory of MEMS Dynamics

A. Deterministic Formulation—Physical Models

Physical-level analysis of electrostatic MEMS requires a self-consistent solution of the coupled mechanical, electrostatic, and fluidic equations. Fig. 1 shows a typical MEMS device—a deformable cantilever beam over a fixed ground plane. When a potential difference is applied between the beam and the ground plane, it induces electrostatic charge on the surface of the conductors. This charge gives rise to an electrostatic pressure acting normal to the surface of the beam, as shown in Fig. 1(a). The surrounding fluid (air), which is at ambient conditions, also exerts a pressure (atmospheric pressure) on the beam. As the beam deforms due to electrostatic pressure, the charge redistributes on the surface of the conductors, and consequently, the electrostatic pressure field changes. At the same time, the displacement of the surrounding fluid due to the deformation of the beam gives rise to fluid damping. The electrostatic and damping forces cause the beam to deform to a state where they are balanced by the internal stiffness and inertial forces at that time instant [see Fig. 1(b)]. This explains the coupling between the mechanical, electrostatic, and fluidic

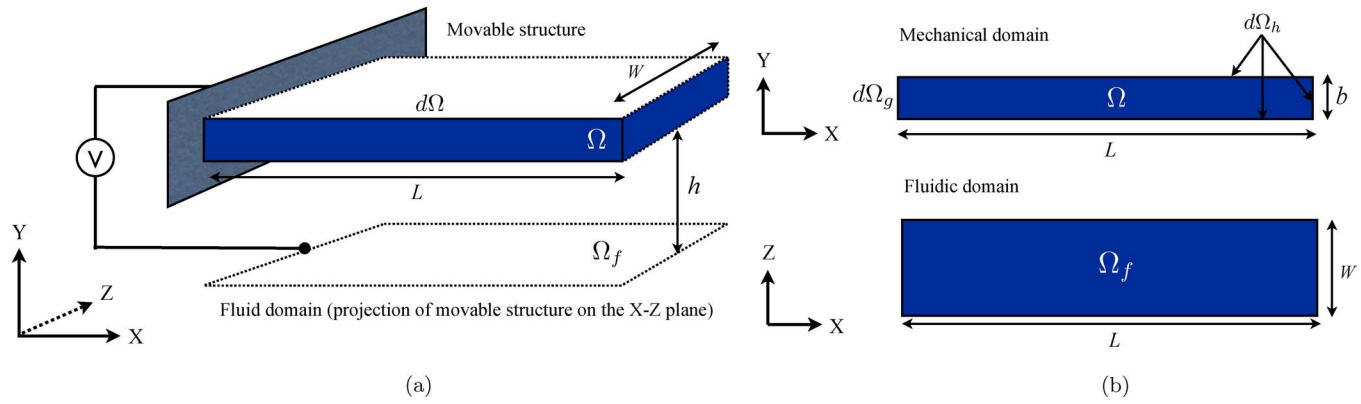

Fig. 2. Computational domain for coupled electromechanical–fluidic problem. (a) Undeformed configuration ($t = 0$). (b) Mechanical and fluidic domains.

energy domains, and a self-consistent solution is required to obtain the final deflection of the beam.

The mechanical deformation of the MEM structures is obtained by performing a transient 2-D geometrically nonlinear elasticity analysis [18]. Let Ω represent the undeformed configuration with boundary $d\Omega = d\Omega_g \cup d\Omega_h$, as shown in Fig. 2. The governing equations for the deformation of the MEM structures in the absence of body force are given as

$$\rho\ddot{\mathbf{u}} = \nabla \cdot (\mathbf{FS}) \quad \text{in } \Omega \tag{1}$$

$$\mathbf{u} = \mathbf{G} \quad \text{on } d\Omega_g \tag{2}$$

$$\mathbf{P} \cdot \mathbf{N} = \mathbf{H} \quad \text{on } d\Omega_h \tag{3}$$

$$\mathbf{u}|_{t=0} = \mathbf{G_0} \quad \text{in } \Omega \tag{4}$$

$$\dot{\mathbf{u}}|_{t=0} = \mathbf{V_0} \quad \text{in } \Omega \tag{5}$$

where $\mathbf{u}$, $\dot{\mathbf{u}}$, and $\ddot{\mathbf{u}}$ are the displacement, velocity, and acceleration vectors, respectively. ρ is the density, $\mathbf{F}$ is the deformation gradient, and $\mathbf{P}$ and $\mathbf{S}$ are the first and second Piola–Kirchoff stress tensors, respectively. Equations (2) and (3) are the displacement and traction boundary conditions, respectively, where $\mathbf{G}$ is the prescribed displacement, $\mathbf{H}$ is the surface traction on the structure due to the electrostatic and fluid pressures, and $\mathbf{N}$ is the unit outward normal vector in the undeformed configuration. Equations (4) and (5) are the initial conditions for displacement and velocity, respectively, where $\mathbf{G_0}$ is the initial displacement and $\mathbf{V_0}$ is the initial velocity. A Newmark scheme with implicit trapezoidal rule is used to solve the nonlinear dynamical system posed in (1)–(5) (see [3] for details).

Electrostatic analysis is required to compute the electrostatic pressure acting on the surface of the microstructures. In the absence of any free charges, the electrostatic potential can be obtained by solving the Laplace equation, given as

$$\frac{\partial^2\phi}{\partial x^2} + \frac{\partial^2\phi}{\partial y^2} = 0 \quad \text{in } \bar{\omega} \tag{6}$$

where ϕ is the potential field in the dielectric medium $\bar{\omega}$ (in the deformed configuration), surrounding the conductors. A Lagrangian boundary integral formulation (see [19] for details) of (6) is used to compute the surface charge density $\sigma(\mathbf{X})$ on the conductors. The electrostatic pressure acting normal to the surface of the conductors, in the deformed configuration, can then be computed from the surface charge density as

$$P_e = \frac{\sigma^2}{2\epsilon} \tag{7}$$

where ϵ is the dielectric constant of the medium.

The fluid damping between the MEM structure and the ground plane is modeled using squeeze film damping. The isothermal compressible Reynold's squeeze film equation is given by [20]

$$\frac{\partial}{\partial x}\left[(1+6K)h^3 P_f \frac{\partial P_f}{\partial x}\right] + \frac{\partial}{\partial z}\left[(1+6K)h^3 P_f \frac{\partial P_f}{\partial z}\right] = 12\eta\frac{\partial(P_f h)}{\partial t} \quad \text{in } \omega_f \tag{8}$$

where h is the gap between the movable structure and the ground electrode, P_f is the fluid pressure, and η is the viscosity of the surrounding fluid. $K = \lambda/h$ is the Knudsen number, where λ is the mean free path of the fluid. Equation (8) is obtained from the Navier–Stokes equation by accounting for slip correction and neglecting the fluid velocity and the variation of all physical quantities in the height (Y) direction. ω_f represents the projection of the deformed MEM structure onto the ground plane. As described in [4], (8) can be solved in the undeformed configuration using an appropriate Lagrangian mapping. As a result, the fluid domain Ω_f, where the Reynold's squeeze film equation is solved, is the projection of the undeformed MEM structure on the $X-Z$ plane, as shown in Fig. 2. The fluid pressure P_f obtained from (8) is integrated along the Z-direction to compute the effective fluid pressure P_{fe}, which is applied as a boundary condition in the 2-D mechanical analysis in the $X-Y$ domain.

The effective fluid pressure P_{fe} from the fluidic analysis and the electrostatic pressure P_e obtained from the electrostatic analysis (7) are used to compute the surface traction $\mathbf{H}$ (3) using

$$\mathbf{H} = J(P_e - P_{fe})\mathbf{F}^{-T}\mathbf{N} \tag{9}$$

where $J = \det(\mathbf{F})$. Equation (9) represents the nonlinear coupling between the mechanical, electrostatic, and fluidic energy

domains. We can represent the coupled system [(1)–(5), (6) and (7), and (8) and (9)] as

$$\mathcal{L}(\mathbf{u}, \sigma, P_f; \mathbf{X}, t) = 0, \qquad (\mathbf{X}, t) \in \Omega \times T \tag{10}$$

such that $t \in [0, T]$ represents the time interval of interest. Such a system can be solved easily using FEM and BEM [21]. A deterministic framework for self-consistent solution of this coupled nonlinear system using relaxation and Newton schemes has been presented in [4].

B. Stochastic Formulation

State-of-the-art design methodologies for MEMS are based on deterministic approaches (as described earlier), where the input parameters such as geometrical and physical properties (denoted as $\boldsymbol{\alpha}$) are assumed to be known precisely. For the given values of the input parameters $\boldsymbol{\alpha}$, one can simply solve the coupled system [given by (10)] for the field variables—displacement, surface charge density, and fluidic pressure—and evaluate relevant quantities of interest (denoted as $\boldsymbol{\beta}$) such as capacitance, resonant frequency, quality factor, etc. For example, for the device shown in Fig. 1, the input parameters and quantities of interest may be given as $\boldsymbol{\alpha} = [E, g]$ and $\boldsymbol{\beta} = [C]$, respectively, where E, g, and C denote Young's modulus, the gap between the electrodes, and the capacitance in the deformed configuration, respectively. By using the given values of input parameters $\boldsymbol{\alpha}$, one can easily compute the quantities of interest $\boldsymbol{\beta}$. However, in practice, such devices may be subjected to severe stochastic variations in these parameters, which must be considered during modeling. To this end, we develop a stochastic modeling framework to quantify the effect of variations in input parameters on relevant quantities of interest. The stochastic modeling approach has two key ingredients which are given as follows.

1) Representation of Input Uncertainty: Uncertainties can be described using stochastic quantities—uncertain parameters can be modeled using random variables, and uncertain spatial or temporal functions are represented as random fields or processes. We assume that all uncertain input parameters $\boldsymbol{\alpha}$ can be characterized using n independent random variables. Let $\boldsymbol{\xi} = \{\xi_i\}_{i=1}^n$ represent mutually independent random variables with images Γ_i and pdfs $\rho_i : \Gamma_i \to \mathbb{R}^+$, for $i = 1, \ldots, n$. Then, the joint pdf $\rho(\boldsymbol{\xi})$ is given as

$$\rho(\boldsymbol{\xi}) = \prod_{i=1}^{n} \rho_i(\xi_i) \qquad \forall\, \boldsymbol{\xi} \in \Gamma \tag{11}$$

where $\Gamma = \prod_{i=1}^n \Gamma_i$ represents the support of the set of random variables.

For example, for the MEMS device considered earlier, the Young's modulus E and gap g can be assumed to vary between $[E_{\min}, E_{\max}]$ and $[g_{\min}, g_{\max}]$, respectively. Given this information, we can model these parameters as uniformly distributed random variables over their given range of variation and can represent them in terms of $\boldsymbol{\xi} = \{\xi_1, \xi_2\}$ as

$$E = E_{\min} + (E_{\max} - E_{\min})\xi_1 \qquad g = g_{\min} + (g_{\max} - g_{\min})\xi_2 \tag{12}$$

where ξ_1 and ξ_2 are mutually independent uniformly distributed random variables in $\Gamma_i = [0, 1]$, $i = 1, 2$. We must remark that the ability to correctly characterize uncertain input parameters in terms of random variables (with appropriate distribution) largely depends on the availability of detailed experimental data regarding these parameters, which, unfortunately, is not the case for most of the MEMS devices. For certain parameters, experiments provide limited information about the variation, in the form of nominal values with error bars. In such a situation, the most straightforward way is to model the uncertain parameter as uniformly distributed random variable over the given range.

2) Uncertainty Propagation: The stochastic formulation treats uncertainty as a separate dimension (in addition to space and time), using which all dependent stochastic variables are represented as multidimensional functions. Specifically, having characterized input uncertain parameters in terms of n independent random variables, all unknown dependent variables (field variables and quantities of interest) can be represented as $(d + n)$-dimensional functions, where d and n refer to the dimensions of the physical space $\Omega \times T$ and stochastic space Γ, respectively. Following this, we seek to quantify the effect of variations in input parameters on dependent variables or, in other words, *propagate* the uncertainty in the input variables to the dependent variables.

To this end, we write the stochastic formulation for the coupled electromechanical–fluidic problem [given by (10)] as follows: We seek the stochastic displacement $\mathbf{u}(\mathbf{X}, t, \boldsymbol{\xi})$, the surface charge density $\sigma(\mathbf{X}, t, \boldsymbol{\xi})$, and the fluidic pressure $P_f(\mathbf{X}, t, \boldsymbol{\xi})$ such that

$$\mathcal{L}(\mathbf{u}, \sigma, P_f; \mathbf{X}, t, \boldsymbol{\xi}) = 0, \qquad (\mathbf{X}, t, \boldsymbol{\xi}) \in \Omega \times T \times \Gamma. \tag{13}$$

Over the years, such a formulation has been employed by researchers in various ways, for the purpose of uncertainty propagation, and is considered next.

III. Uncertainty Propagation

The computational methods available for uncertainty propagation can be broadly classified into two major categories—methods based on a statistical approach and methods based on a nonstatistical approach. The statistical approach includes methods such as MC simulations and various sampling schemes such as stratified sampling, Latin hypercube sampling (LHS), etc. These statistical methods are straightforward to implement, but can be computationally expensive, as their accuracy depends on the sample size. The most popular of the nonstatistical methods are based on techniques which seek to directly *discretize* the unknown stochastic solution. One such approach is based on a spectral discretization technique—*GPC* [13], [22]—which employs orthogonal polynomials to represent the unknown stochastic solution. Although this approach provides high accuracy and fast convergence, its implementation is nontrivial and requires substantial code modification (see [13] for details). Another nonstatistical method in this class, which has recently received much attention, is known as the *SC method*. The stochastic modeling framework developed in this paper is based on the SC approach. In this section, we briefly

review the MC method and describe the SC approach in the context of stochastic modeling of MEMS.

A. MC Method

The MC method has been used traditionally for systems with random input parameters. It involves generating various realizations of the input parameters according to the underlying probability distribution and repeatedly employing the deterministic solver for each realization. Equation (13) can be easily solved using the MC method as follows.

1) For the given number of realizations N, generate independent and identically distributed (i.i.d.) random variables $\{\boldsymbol{\xi}^j\} = [\xi_1^j, \ldots, \xi_n^j]$, for $j = 1, \ldots, N$.
2) For each of the realizations, solve the deterministic problem $\mathcal{L}(\mathbf{u}^j, \sigma^j, P_f^j; \mathbf{X}, t, \boldsymbol{\xi}^j) = 0$ and obtain the field variables $(\mathbf{u}^j, \sigma^j, P_f^j)$ and quantities of interest $\boldsymbol{\beta}^j$, for $j = 1, \ldots, N$.
3) Compute the required statistics such as mean μ and variance ν, for example,

$$\mu(\mathbf{u}) = \frac{1}{N}\sum_{j=1}^{N} \mathbf{u}^j \qquad \nu(\mathbf{u}) = \frac{1}{N}\sum_{j=1}^{N} \left(\mathbf{u}^j - \mu(\mathbf{u})\right)^2. \quad (14)$$

The MC method only requires a working deterministic code and readily generates the required statistics. The amount of work required for an MC simulation to converge to a given accuracy $\bar{\epsilon}$ is $\bar{\epsilon}(N) = \mathcal{O}(N^{-1/2})$, which is independent of the number of random dimensions n. Although the MC method is highly scalable (as its convergence does not depend on n) and straightforward to implement, it offers slow convergence rate. Thus, for complex multiphysics MEMS problems, based on high-fidelity computational models, it often becomes impractical due to prohibitive computational cost. The convergence of the MC method can be improved by using techniques such as the LHS [23], the quasi-MC method [24], the Markov chain–MC method [25], etc. As mentioned before, several researchers have used MC simulations to consider the uncertainty associated with various input parameters during the design of electrostatic MEMS [5]–[8].

B. SC Method

In recent years, there has been a growing interest in another class of methods known as the SC method [14]–[16]. Since its introduction, it has been successfully applied to various problems such as natural convection [15], fluid flow [26], etc. The basic idea of the SC approach is to approximate the unknown stochastic solution by a polynomial interpolation function in the multidimensional random space. The interpolation is constructed by solving (sampling) the deterministic problem at a *predetermined* set of points $\Theta_N = \{\boldsymbol{\xi}^i\}_{i=1}^N$. The set of nodes Θ_N is chosen as the sparse grid points generated using the Smolyak algorithm [17], unlike the MC approach where the sampling points are chosen in a statistical manner. For completeness, a brief review of the sparse grid interpolation procedure based on the Smolyak algorithm is presented in the Appendix.

By using the sparse grid interpolation, the approximate displacement $\hat{\mathbf{u}}(\mathbf{X}, t, \boldsymbol{\xi})$, surface charge density $\hat{\sigma}(\mathbf{X}, t, \boldsymbol{\xi})$, and fluid pressure $\hat{P}_f(\mathbf{X}, t, \boldsymbol{\xi})$ can be written as

$$\left[\hat{\mathbf{u}}(\mathbf{X}, t, \boldsymbol{\xi}), \hat{\sigma}(\mathbf{X}, t, \boldsymbol{\xi}), \hat{P}_f(\mathbf{X}, t, \boldsymbol{\xi})\right] = \sum_{i=1}^{N} \left[\mathbf{u}(\mathbf{X}, t, \boldsymbol{\xi}^i), \sigma(\mathbf{X}, t, \boldsymbol{\xi}^i), P_f(\mathbf{X}, t, \boldsymbol{\xi}^i)\right] L_i(\boldsymbol{\xi}) \quad (15)$$

where $\{L_i\}_{i=1}^N$ are the interpolation basis functions such that $L_i(\boldsymbol{\xi}^j) = \delta_{ij}$. By using this interpolation in (13), the collocation procedure gives

$$\mathcal{L}(\hat{\mathbf{u}}, \hat{\sigma}, \hat{P}_f; \mathbf{X}, t, \boldsymbol{\xi})|_{\boldsymbol{\xi}^k} = 0 \qquad \forall\, k \in 1, \ldots, N. \quad (16)$$

By using the property of the interpolation polynomials $L_i(\boldsymbol{\xi}^j) = \delta_{ij}$, this immediately leads to, for $k = 1, \ldots, N$,

$$\mathcal{L}\left(\mathbf{u}(\mathbf{X}, t, \boldsymbol{\xi}^k), \sigma(\mathbf{X}, t, \boldsymbol{\xi}^k), P_f(\mathbf{X}, t, \boldsymbol{\xi}^k); \mathbf{X}, t, \boldsymbol{\xi}^k\right) = 0, \quad (\mathbf{X}, t) \in \Omega \times T. \quad (17)$$

Thus, the SC procedure reduces to solving N deterministic systems, at each nodal point $\boldsymbol{\xi}^k$, $k = 1, \ldots, N$, in a given set of points Θ_N. We note that, using the deterministic solution at a few collocation points, the entire stochastic solution can be constructed [as given by (15)]. For example, the deformation at any point $\boldsymbol{\xi} \in \Gamma$ in the random domain is simply given as $\hat{\mathbf{u}}(\mathbf{X}, t, \boldsymbol{\xi})$. In addition to the field variables, the quantities of interest $\boldsymbol{\beta}$ can also be approximated as

$$\hat{\boldsymbol{\beta}}(\boldsymbol{\xi}) = \sum_{i=1}^{N} \boldsymbol{\beta}^i L_i(\boldsymbol{\xi}) \quad (18)$$

where $\boldsymbol{\beta}^i$ denotes the quantities of interest for the set of input parameters corresponding to $\boldsymbol{\xi}^i$.

The statistics of the random solution, such as mean $\mu(\cdot)$ and variance $\nu(\cdot)$, can be computed as

$$\mu(\mathbf{u})(\mathbf{X}, t) = \sum_{i=1}^{N} \mathbf{u}(\mathbf{X}, t, \boldsymbol{\xi}^i) w_i \quad (19)$$

$$\nu(\mathbf{u})(\mathbf{X}, t) = \sum_{i=1}^{N} \left(\mathbf{u}(\mathbf{X}, t, \boldsymbol{\xi}^i) - \mu(\mathbf{u})\right)^2 w_i,$$

$$w_i = \int_{\Gamma} L_i(\boldsymbol{\xi}) \rho(\boldsymbol{\xi})\, \mathrm{d}\boldsymbol{\xi} \quad (20)$$

where $\rho(\boldsymbol{\xi})$ represents the joint pdf of the random variables $\boldsymbol{\xi}$ and $\{w_i\}_{i=1}^N$ are the weights which can be precomputed and stored for later use. The complexity of the sparse grid collocation approach is given as

$$\bar{\epsilon}(N) = \mathcal{O}\left(N^{-r}(\log_2 N)^{(r+2)(n-1)+1}\right) \quad (21)$$

for solutions with bounded mixed derivatives up to order r. Thus, for sufficiently smooth functions, this approach would

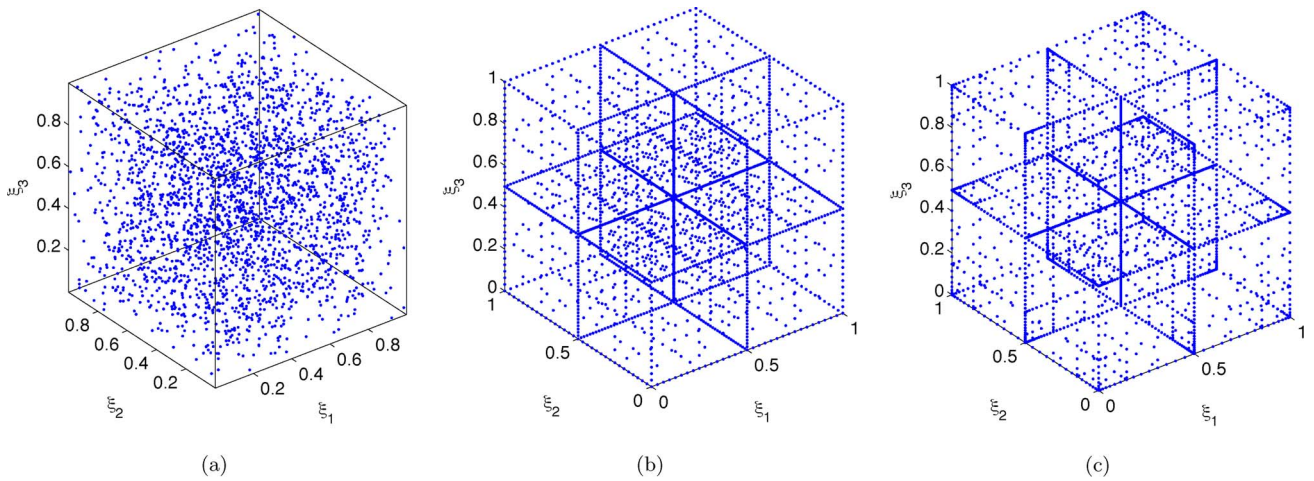

Fig. 3. Illustration of node distributions used for MC simulations and sparse grid interpolation (see the Appendix for details regarding generation of sparse grids). (a) MC grid. (b) Sparse grid obtained using piecewise linear basis functions based on equidistant nodes. (c) Sparse grid obtained using Lagrange polynomials based on Chebyshev nodes.

be orders of magnitude faster than the MC method. In addition to the faster convergence rate, the fact that the procedure only requires solving the deterministic problem at a set of sample points makes the implementation straightforward. The advantages of this approach, in the context of stochastic modeling of MEMS, can be summarized as follows.

1) This approach only requires applying the previously validated high-fidelity computational models (such as FEM–BEM models described in Section II) at a predetermined set of support nodes. Thus, unlike the *intrusive* GPC-based framework, which requires significant code modification, the stochastic implementation for this approach is simply developed as a *wrapper* around the already existing deterministic code.
2) For the number of uncertain parameters, one usually needs to consider for the analysis of electrostatic MEMS; this approach is orders of magnitude faster than the MC method to obtain the same level of accuracy.
3) Unlike the MC method, this approach constructs the entire stochastic solution by sampling of deterministic solution at a few nodes. This explicit representation of the dependent variables in terms of the input parameters can be used for a variety of useful purposes such as follows.
   a) The solution can be visualized in the stochastic domain, revealing important information about the behavior of the dependent variable with respect to each uncertain parameter.
   b) In addition to moments such as mean and variance, the entire pdf can be obtained, which can be used to compute failure probabilities, etc.
   c) The sensitivities can be effectively computed, which can be used to identify critical design parameters, as would be demonstrated through numerical examples.

We illustrate the grids obtained by generating independent uniformly distributed random variables (for MC) and sparse node distributions using piecewise linear and Lagrange polynomials for a 3-D $(n = 3)$ problem in Fig. 3. We also note that the numerical results presented in this paper are obtained using sparse grids based on piecewise linear basis functions with equidistant nodes. The SC method has been detailed in Algorithm 1.

Algorithm 1 Stochastic collocation method

1: Preprocessing Identify uncertain parameters (material properties and geometrical parameters) and represent them in terms of independent random variables $\boldsymbol{\xi} = [\xi_1, \xi_2, \ldots, \xi_n]^{\mathrm{T}}$, such that n represents the dimension of the random domain Γ.

2: Sparse grid interpolation Construct the multidimensional interpolation as follows:

a. *Sparse grid:* Generate the set of sparse grid nodes $\Theta_N = \{\boldsymbol{\xi}^j\}_{j=1}^N$ using the Smolyak algorithm based on an appropriate 1-D interpolation rule.

b. *Sampling:* For each of the nodes $\{\boldsymbol{\xi}^j\}$, solve the deterministic problem $\mathcal{L}(\mathbf{u}^j, \sigma^j, P_f^j; \mathbf{X}, t, \boldsymbol{\xi}^j) = 0$ and obtain the field variables $(\mathbf{u}^j, \sigma^j, P_f^j)$ and quantities of interest $\boldsymbol{\beta}^j$, for $j = 1, \ldots, N$.

c. *Interpolation:* Construct the interpolant for the dependent variables using the sampled values, e.g., $\hat{\mathbf{u}}(\mathbf{X}, t, \boldsymbol{\xi}) = \sum_{j=1}^N \mathbf{u}(\mathbf{X}, t, \boldsymbol{\xi}^j) L_j(\boldsymbol{\xi})$, where $\{L_j(\boldsymbol{\xi})\}_{j=1}^N$ are the interpolation basis functions.

3: Postprocessing

a. *Computation of moments:* Compute the required statistics, such as mean and variance, using $\mu(\mathbf{u})(\mathbf{X}, t) = \sum_{j=1}^N \mathbf{u}(\mathbf{X}, t, \boldsymbol{\xi}^j) w_j$ and $\nu(\mathbf{u})(\mathbf{X}, t) = \sum_{j=1}^N (\mathbf{u}(\mathbf{X}, t, \boldsymbol{\xi}^j) - \mu(\mathbf{u}))^2 w_j$, respectively, where $w_j = \int_\Gamma L_j(\boldsymbol{\xi}) \rho(\boldsymbol{\xi}) \, \mathrm{d}\boldsymbol{\xi}$ are the weights, which can be precomputed.

b. *Probability Density Function (pdf):* For $N_{\mathrm{mc}} \gg N$, generate i.i.d. random variables $\{\boldsymbol{\eta}^j\}$ and evaluate the interpolant $\hat{\mathbf{u}}^j = \hat{\mathbf{u}}(\mathbf{X}, t, \boldsymbol{\eta}^j)$, $j = 1, \ldots, N_{\mathrm{mc}}$. Use the set of values $\{\hat{\mathbf{u}}^j\}_{j=1}^{N_{\mathrm{mc}}}$ to construct the required pdf.

IV. Numerical Results

In this section, we present a few numerical examples to demonstrate the SC approach toward quantifying the effect of stochastic variations in input parameters on device performance and identification of critical design parameters. Specifically,

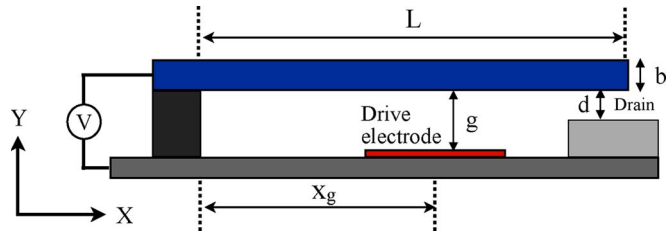

Fig. 4. Electrostatically actuated MEMS switch [27].

TABLE I
UNCERTAIN DESIGN PARAMETERS FOR MEMS SWITCH

Design parameter	Nominal value	Variation
Young's modulus (E) [GPa]	207	10%
Length (L) [μm]	70	2%
Beam thickness (b) [μm]	2.0	10%
Gap (g) [μm]	1.5	10%
Location of drive electrode (x_g) [μm]	35	2%

we consider two devices—MEMS switch and resonator—and study the effect of variations in Young's modulus and various geometrical parameters on relevant quantities of interest, such as actuation behavior, resonant frequency, and quality factor.

We also show that the SC approach can be effectively used to identify critical design parameters, that lead to higher variability in the device performance. These parameters can then be controlled during fabrication in order to meet the prescribed design criterion with the desired confidence level.

A. Dynamic Analysis of a MEMS Switch

We consider the transient response of an electrostatically actuated MEMS switch [27], which is modeled by a cantilever beam of length L, thickness b, and width $W = 30$ μm, as shown in Fig. 4. The tip height is $d = 0.75$ μm (above the drain), and the beam is initially at a height g above the drive electrode and the substrate and is fabricated from gold-plated nickel with Young's modulus E and density $\rho = 8900$ kg/m^3. The drive electrode of length 28 μm is placed such that its center is located at a distance x_g from the fixed end of the beam. A potential difference V is applied between the beam and the drive electrode.

Given the set of uncertain design parameters $\boldsymbol{\alpha} = [E, L, b, g, x_g]$, we wish to quantify the effect of uncertainty in these parameters on relevant quantities of interest. For this example, we are interested in two output parameters $\boldsymbol{\beta} = [Y_s, T_s]$, where Y_s represents the equilibrium vertical tip displacement of the beam corresponding to a step voltage $V_1 = 100$ V and T_s denotes the time taken by the beam to strike against the drain for a step voltage $V_2 = 200$ V. We assume that the uncertain parameters $\boldsymbol{\alpha}$ are uniformly distributed random variables with nominal values given by $\boldsymbol{\alpha}_0 = [207$ GPa, 70 μm, 2 μm, 1.5 μm, 35 μm$]$ and fraction of variation around the nominal values given by $\Delta\boldsymbol{\alpha} = [0.1, 0.02, 0.1, 0.1, 0.02]$, as tabulated in Table I. This implies, for example, that the thickness of the beam and the gap between

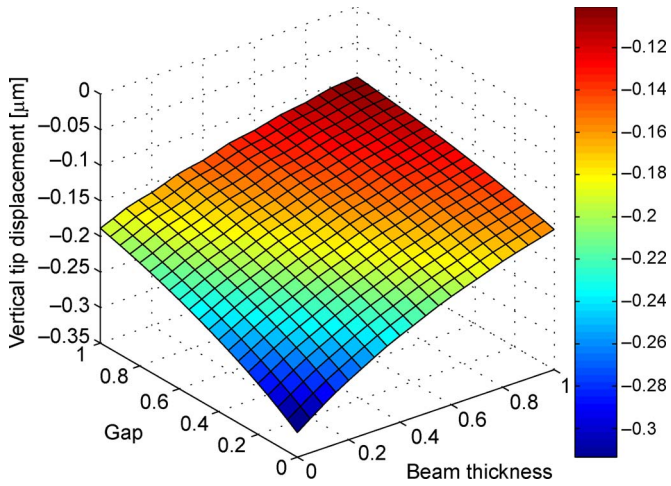

Fig. 5. Vertical tip deflection as a function of beam thickness and gap parameters.

electrodes are assumed to be uniformly distributed random variables between $[1.8$ μm, 2.2 μm$]$ and $[1.35$ μm, 1.65 μm$]$, respectively. The uncertain parameters $\boldsymbol{\alpha}$ are represented in terms of random variables $\boldsymbol{\xi} = \{\xi_i\}_{i=1}^5$, where ξ_i, $i = 1, \ldots, 5$, are mutually independent uniformly distributed random variables in [0, 1]. We employ the sparse grid interpolation procedure (as described in Algorithm 1) to approximate the vertical tip deflection and the strike time as a function of the input parameters. In Fig. 5, we plot the vertical tip deflection as a function of the beam thickness and gap parameters (varying between [0, 1], such that values 0 and 1 correspond to minimum and maximum gap or thickness value, respectively) while fixing the remaining input variables at their respective nominal values. As expected, lower values of gap and beam thickness lead to higher tip deflection.

1) Worst Case Behavior: In order to gauge the variability in the switch performance corresponding to the assumed variation in the input parameters, we first consider the worst case behavior of the switch. In Fig. 6(a), we plot the transient response of the beam tip corresponding to a step voltage $V = 100$ V, for mean and extreme values of the input parameters, obtained using the deterministic solver. As can be easily seen, the parameters $\boldsymbol{\alpha} = \boldsymbol{\alpha}_1$ and $\boldsymbol{\alpha}_2$ represent the worst case scenarios and also indicate the extent of variation in the actuation behavior of the switch corresponding to the variation in the design parameters. Clearly, for $\boldsymbol{\alpha} = \boldsymbol{\alpha}_1$, the beam deflects much closer to the substrate, resulting in higher squeeze film damping, as opposed to the case $\boldsymbol{\alpha} = \boldsymbol{\alpha}_2$. Similarly, we plot the transient response of the beam for mean and extreme values of the parameters for $V = 200$ V in Fig. 6(b).

The vertical tip displacement Y_s and the strike time T_s vary from -0.39 to -0.1 μm and from 0.67 to 1.21 μs, respectively. In the absence of any other information about these quantities of interest, one may be forced to design for the worst case scenario, which may lead to over conservative designs. The SC procedure can be used to estimate statistics and pdfs of these quantities of interest, which can then be used to compute important information such as failure probabilities, etc., leading to more effective and reliable designs. We must note that, for

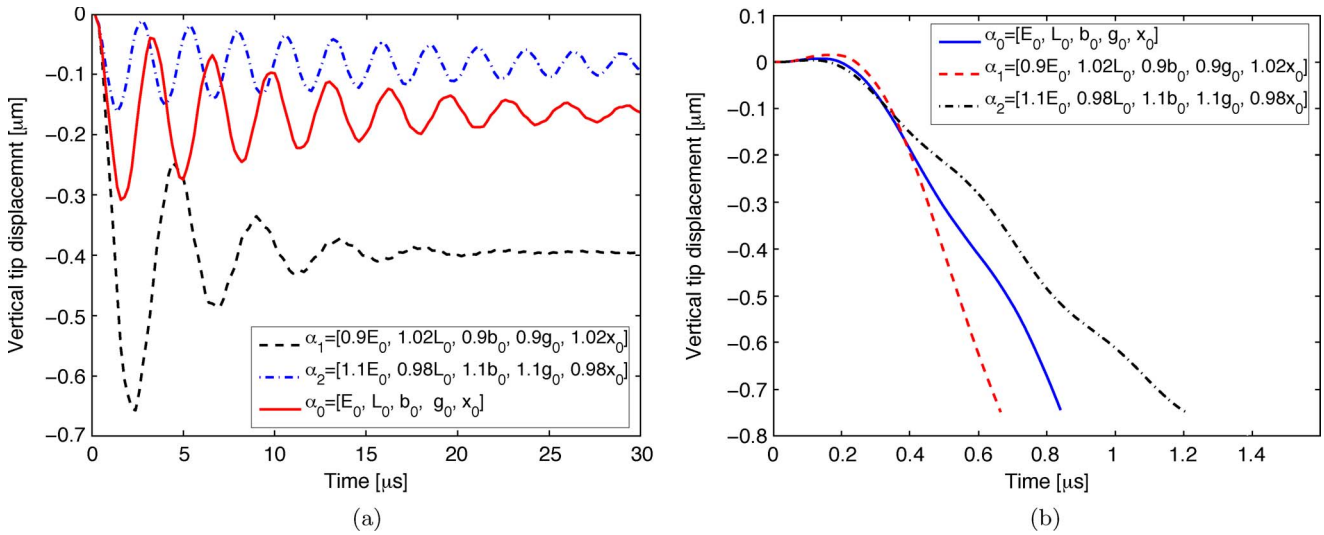

(a) (b)

Fig. 6. Worst case behavior: Transient response of the beam tip corresponding to a step voltage V. (a) $V = 100$ V. (b) $V = 200$ V.

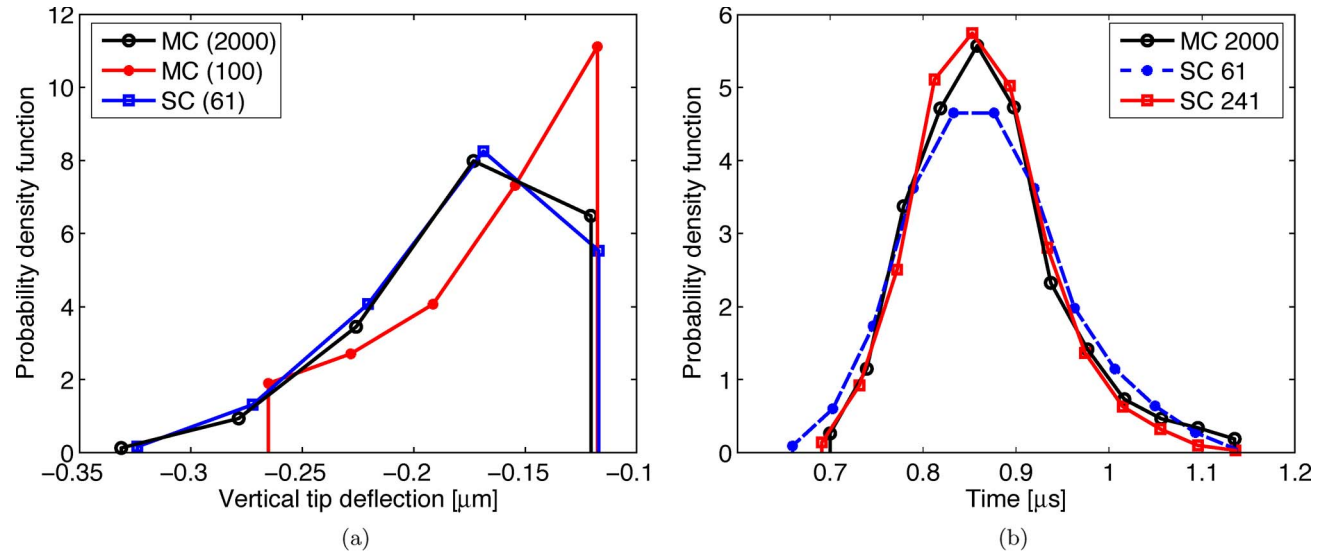

(a) (b)

Fig. 7. Comparison between pdfs of output parameters obtained using MC simulations and SC approach. (a) PDF of vertical tip deflection at $V = 100$ V. (b) PDF of strike time at $V = 200$ V.

situations involving higher number of uncertain parameters, it may not always be a trivial exercise to obtain information even about the worst case device behavior. In such situations, the interpolant constructed for the unknown solution during the SC procedure can also be effectively used to estimate the variability in the device performance, in addition to estimating the statistics.

2) Verification Using MC Simulations: The results obtained using the SC approach are verified using rigorous MC simulations. We conducted several numerical experiments and determined that MC simulations converge for 2000 samples and hence use those results for verification. In Fig. 7(a) and (b), we plot the pdfs for the vertical tip displacement and the strike time obtained using MC simulations and the SC approach. As can be seen, the distribution obtained using the SC approach based on only a few sampling points (61 and 241 for deflection and strike time, respectively) agrees reasonably well with the MC results obtained using 2000 sampling nodes. In Fig. 7(a), we also plot the pdf for vertical tip displacement obtained using MC simulations based on merely 100 samples, which demonstrates that MC simulations based on few realizations may lead to inaccurate results. The mean and standard deviation values for tip displacement and strike time are tabulated in Table II.

TABLE II
MEAN AND STANDARD DEVIATION FOR VERTICAL TIP DEFLECTION AND STRIKE TIME USING MC AND SC APPROACH

	Vertical tip deflection Y_s $[\mu m]$		Strike time T_s $[\mu s]$	
	MC (2000)	SC (61)	MC (2000)	SC (241)
Mean	-0.1712	-0.1735	0.8676	0.8619
SD	0.0446	0.0450	0.08	0.07

3) Sensitivity Analysis: In addition to quantifying the effect of uncertain parameters on the performance of the switch, we

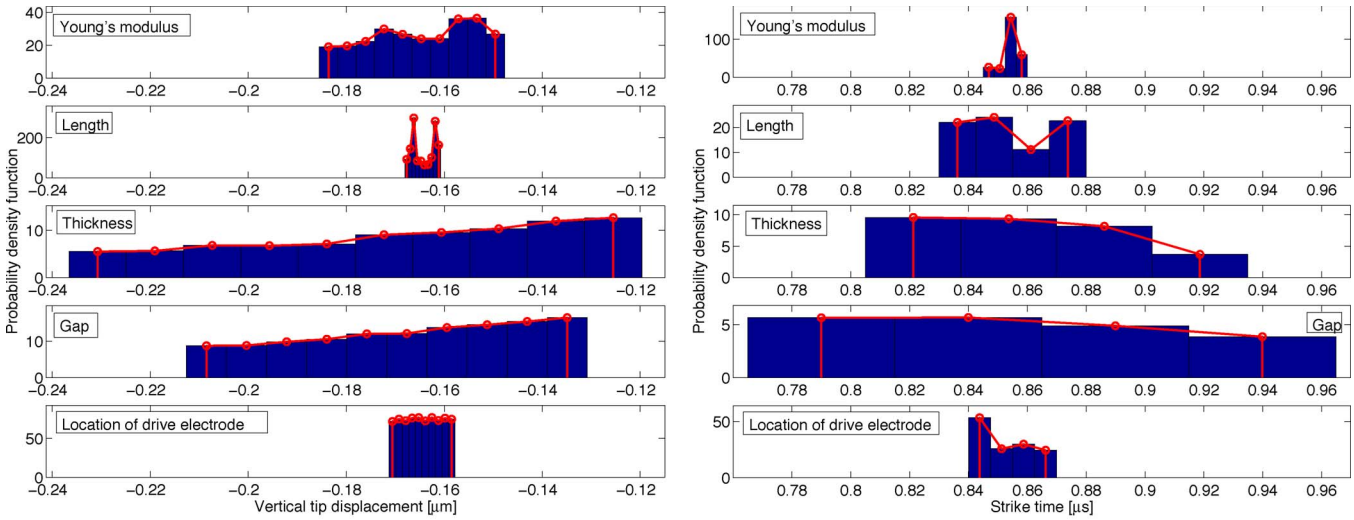

Fig. 8. Sensitivity analysis: PDF of important output parameters w.r.t. each uncertain input parameter (other parameters are fixed at their respective nominal values). (a) PDF of vertical tip deflection. (b) PDF of strike time.

also wish to identify critical design parameters, which can be controlled during fabrication, in order to obtain desirable performance. For example, we assume that one needs to design a switch such that the vertical tip deflection lies between -0.25 and -0.11 μm and that the strike time is less than 1 μs. The pdfs for tip deflection and strike time in Fig. 7(a) and (b), respectively, indicate that, for the given variation in the parameters, such a design criterion is not satisfied. In the absence of any information regarding the relative importance of each parameter, one might be forced to prescribe tighter tolerances for all the parameters in order to meet the design criterion. However, since the SC approach results in explicit expressions for the quantities of interest in terms of design variables, we can measure the relative importance of each variable. We recall that the quantities of interest $\boldsymbol{\beta}$ are approximated as [as given by (18)]

$$\hat{\boldsymbol{\beta}}(\boldsymbol{\xi}) = \sum_{i=1}^{N} \boldsymbol{\beta}^i L_i(\xi_1, \ldots, \xi_5) \tag{22}$$

where $\{L_i\}_{i=1}^{N}$ are the interpolation basis function and N is the total number of sparse grid nodes. In order to gauge the relative importance of the kth parameter, we fix all other parameters $\xi_i, \forall\, i \neq k$, at their nominal values and generate the pdf of the quantities of interest by evaluating (22) for realizations of ξ_k.

By using this procedure, in Fig. 8(a), we plot the pdf for vertical tip deflection with respect to each uncertain input parameter, while other parameters are fixed at their nominal values. As can be clearly seen, the uncertainty in beam thickness and gap between the electrodes leads to more variation in the tip deflection, as compared to the uncertainty in Young's modulus, beam length, and location of the drive electrode. In fact, the variation in beam length seems to have no significant effect on the vertical tip deflection. Fig. 8(b) shows that the variations in beam thickness and gap are also responsible for high variability in the strike time. It is also interesting to note that the Young's modulus does not have any significant effect on the strike time.

Having identified the beam thickness and gap as the two most critical parameters, we plot the pdfs for tip deflection and strike time in Fig. 9(a) and (b), respectively. We vary the level of uncertainty in these two important parameters as 10%, 7.5%, and 5% while keeping it fixed (same uncertainty as before) for others. It must be noted that, for this purpose, we only need to employ the already constructed interpolant for the quantities of interest and that no additional sampling is required. From this, we can conclude that the beam thickness and gap are two critical parameters for given quantities of interest, and if one could restrict the variation in these two parameters to within 5% of their nominal values, it can be guaranteed that the switch meets the prescribed design criterion. This example demonstrates that the SC approach can be effectively used to quantify the effect of uncertain parameters and also identify critical design variables, leading to reliable and efficient MEMS devices.

B. MEMS Resonator

MEMS resonators have been used in widespread applications such as accelerometers, inertial sensors, RF filters, and oscillators. These devices consist of microstructures subjected to a harmonic potential difference, which causes the structures to vibrate at the frequency of the applied signal. In many applications, the resonant frequency and quality factor are the key performance parameters which need to be predicted accurately. The uncertainty in input parameters may lead to large variations in these key parameters which may effect the performance of these devices. Thus, in order to design reliable MEMS resonators, we need to quantify the effect of uncertain input parameters on the resonant frequency and quality factor.

We consider a doubly clamped beam of length $L = 80$ μm, thickness b, and width $W = 10$ μm, located at a distance g from the ground plane. The beam is assumed to be made of polysilicon with Young's modulus E, and Poisson's ratio is set to be 0.3. As in the previous example, we denote the set of

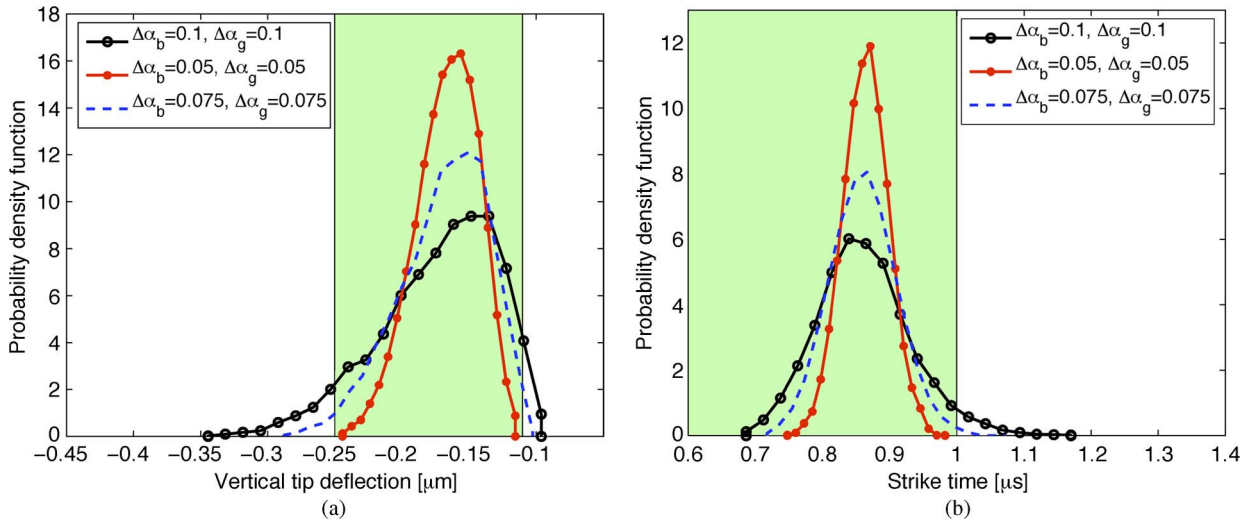

Fig. 9. Illustration of design under uncertainties: PDF and desired range of variation (shaded region) for important output parameters for various levels of input uncertainty. (a) PDFs for vertical tip deflection. (b) PDFs for strike time.

TABLE III
UNCERTAIN DESIGN PARAMETERS FOR MEMS RESONATOR

Design parameter	Nominal value	Variation
Young's modulus (E) $[GPa]$	169	10%
Beam thickness (b) $[\mu m]$	1.0	10%
Gap (g) $[\mu m]$	1.0	10%

uncertain parameters as $\boldsymbol{\alpha} = [E, b, g]$, assumed to be uniformly distributed random variables with nominal values given by $\boldsymbol{\alpha}_0 = [169\ \text{GPa}, 1\ \mu\text{m}, 1\ \mu\text{m}]$ with 10% variation around the nominal values, as listed in Table III. We first apply a step dc bias ($V_{\text{dc}} = 50.0$ V), and once the beam reaches steady state, we apply an additional ac bias signal with amplitude $V_{\text{ac}} = 5.0$ V and frequency $f_d = 1.33$ MHz. For this example, we are interested in quantifying the effect of uncertain design variables on the resonant frequency (f_0) and quality factor (Q) at $V = V_{\text{dc}}$, and the amplitude of the maximum vertical displacement (A) corresponding to $V = V_{\text{dc}} + V_{\text{ac}} \sin(2\pi f_d t)$ at steady state.

In Fig. 10, we plot the transient response of the beam for mean and extreme values of the uncertain input parameters. We can observe that the variation in input parameters leads to significant variation in the response of the beam to pure dc bias, which determines the resonant frequency and the quality factor, as well as the response to combined dc and ac bias, which determines the amplitude of the output signal. This variation in important output parameters may have significant effect on the performance of the resonator.

The quality factor Q of the device is related to the damping ratio τ as $Q = 1/2\tau$, which can be computed by observing the decaying time response of the beam corresponding to the step dc bias. In Fig. 11(a), we plot the damping ratio as a function of beam thickness and gap parameters (varying between [0, 1], such that values 0 and 1 correspond to minimum and maximum gap or thickness value, respectively). As expected, lower values

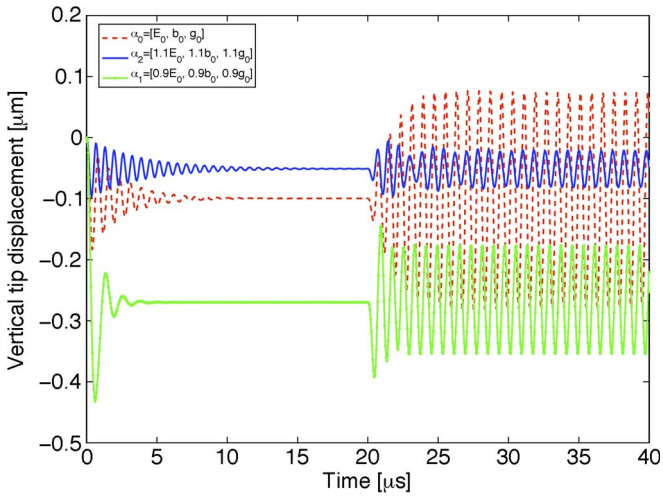

Fig. 10. Transient response of the doubly clamped beam corresponding to a voltage signal $V = V_{\text{dc}}$ for $t \leq 20$ μs and $V = V_{\text{dc}} + V_{\text{ac}} \sin(2\pi f_d t)$ for $t > 20$ μs, where $V_{\text{dc}} = 50.0$ V, $V_{\text{ac}} = 5.0$ V, and $f_d = 1.33$ MHz.

of gap between the electrodes and beam thickness lead to higher squeeze film damping effect. The pdfs for the damping ratio τ obtained using MC simulations (based on 1000 samples) and the SC approach are plotted in Fig. 11(b), which shows a reasonable agreement. In Fig. 12(a) and (b), we plot the pdfs for the resonant frequency f_0 and the amplitude of the output signal A using MC simulations and the SC approach. The mean and standard deviation for the quantities of interest are given in Table IV.

In order to identify the parameters that are critical to resonator performance, we plot the pdfs for resonant frequency and amplitude with respect to each uncertain input parameter, while other parameters are fixed at their nominal values, in Fig. 13(a) and (b), respectively. As can be seen, the beam thickness is the most important parameter as it leads to maximum variation in the output parameters and hence should be controlled during fabrication. We must note (from Fig. 13(a) bottom) that the variation in the gap between the electrodes

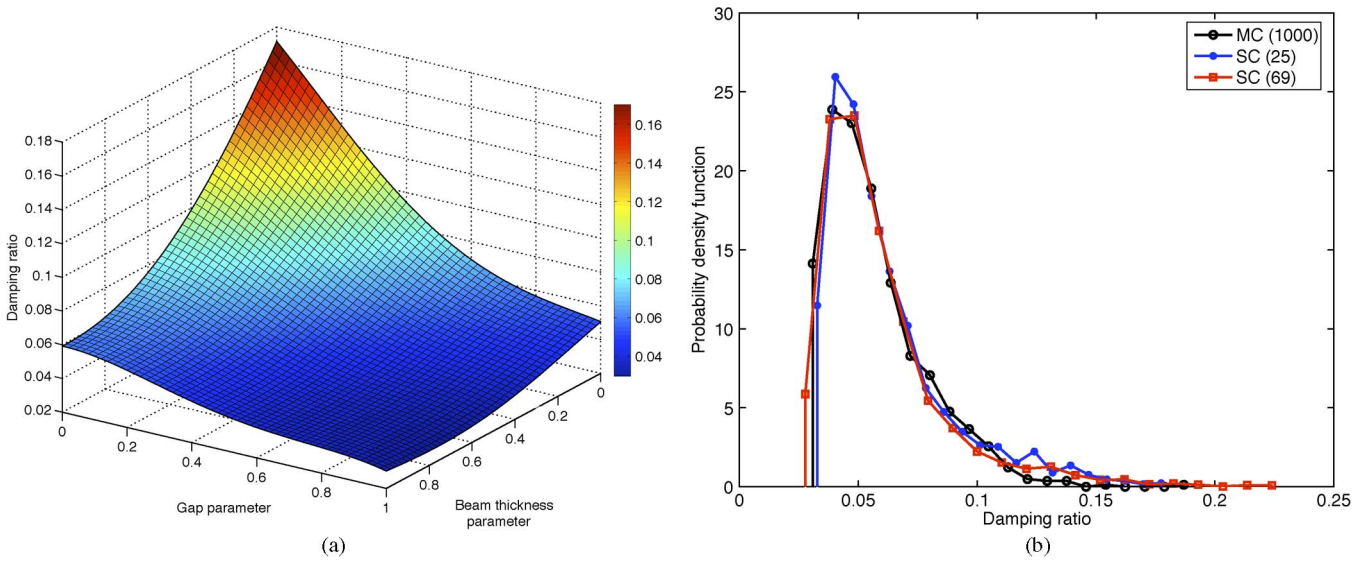

Fig. 11. Damping ratio for the MEMS resonator at $V = V_{\rm dc} = 50$ V. (a) Damping ratio as a function of beam thickness b and gap g parameters, $E = E_0$. (b) PDF of damping ratio obtained using MC simulations and SC approach.

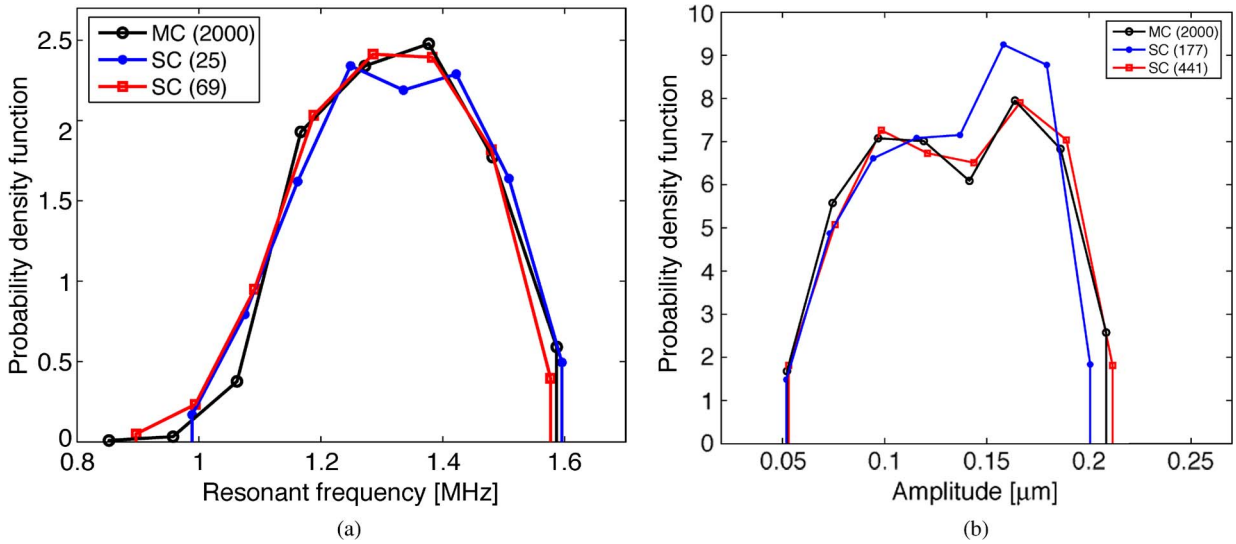

Fig. 12. Comparison between pdfs of output parameters obtained using MC simulations and SC approach. (a) PDF of resonant frequency. (b) PDF of amplitude of output signal.

TABLE IV
MEAN AND STANDARD DEVIATION FOR OUTPUT PARAMETERS

	Damping ratio (τ)		Resonant frequency f_0 $[MHz]$		Amplitude A $[\mu m]$	
	MC (1000)	SC (69)	MC (2000)	SC (69)	MC (2000)	SC (441)
Mean	0.057	0.058	1.329	1.330	0.134	0.130
SD	0.023	0.026	0.12	0.13	0.039	0.04

leads to some variation in the resonant frequency due to the nonlinear nature of the electrostatic force, demonstrating *spring softening* effect in MEMS resonators. As mentioned before, unlike MC simulations, the SC approach leads to explicit expressions for output parameters in terms of the input design variables, which can be used for further analysis. For example, we plot the resonant frequency and the amplitude of the output signal (A) as a function of Young's modulus and beam thickness parameters for various values of the gap between electrodes in Fig. 14. This reveals the correspondence between the resonant frequency of the beam and the output amplitude, since the values of design variables (E, b), which

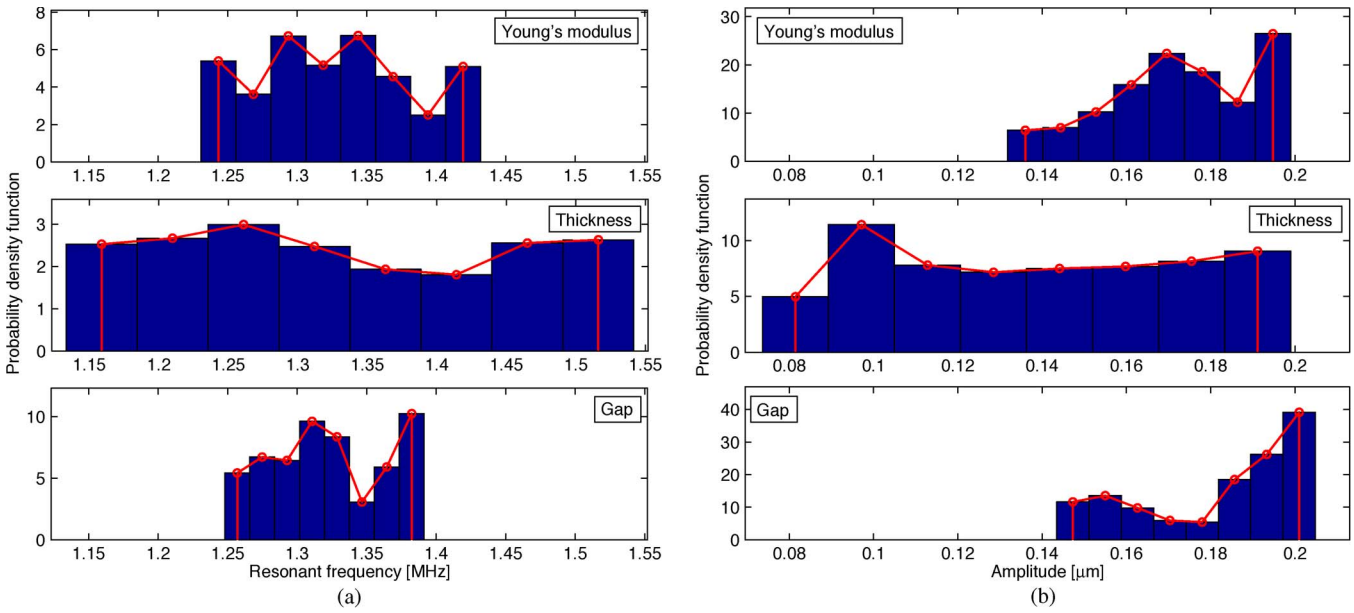

Fig. 13. Sensitivity analysis: PDF of important output parameters w.r.t. each uncertain input parameter (other parameters are fixed at their respective nominal values). (a) PDF of resonant frequency. (b) PDF of amplitude of the output signal.

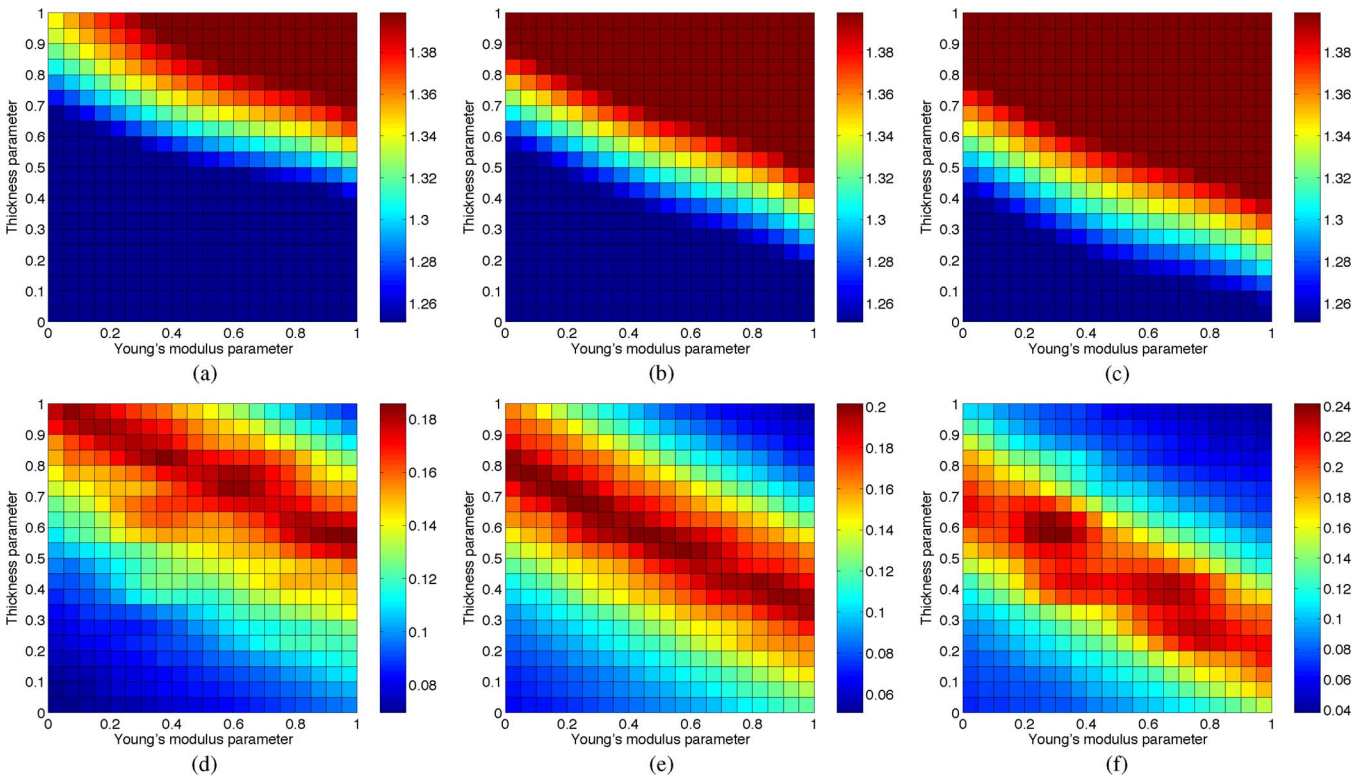

Fig. 14. Plots of (top) resonant frequency and (bottom) amplitude of output signal with Young's modulus and beam thickness parameters for various gap values. (a) Resonant frequency ($g = 0.9$ μm). (b) Resonant frequency ($g = 1.0$ μm). (c) Resonant frequency ($g = 1.1$ μm). (d) Amplitude ($g = 0.9$ μm). (e) Amplitude ($g = 1.0$ μm). (f) Amplitude ($g = 1.1$ μm).

result in resonant frequencies close to the driving frequency $f_d = 1.33$ MHz, also lead to higher values of the amplitude, as can be seen from Fig. 14.

V. Conclusion

This paper has presented an efficient stochastic modeling framework for quantifying the effect of stochastic variations in various design parameters on the performance of electrostatic MEMS devices. The proposed approach approximates the dependent stochastic variables using sparse grid interpolation, which is then used to compute important information such as statistics, probability distribution, and sensitivities of relevant quantities of interest with respect to each of the design variables. The uncertainty quantification information can be effectively used to identify critical design parameters, which

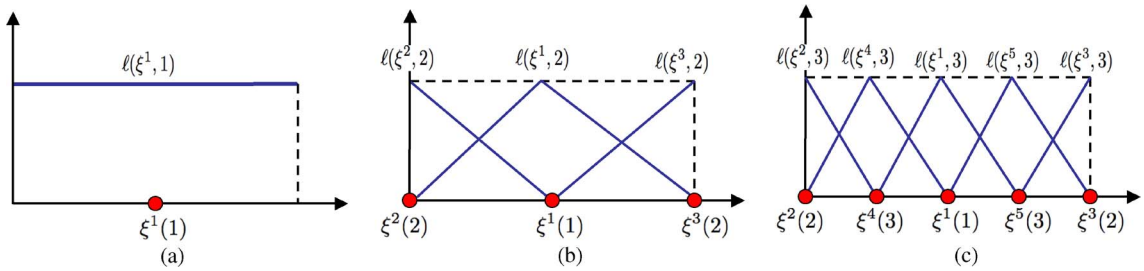

Fig. 15. Univariate piecewise linear interpolation basis functions and support nodes at various levels of interpolation. Numbers in parenthesis denote the corresponding depth coordinate for each node. (a) $p = 1$. (b) $p = 2$. (c) $p = 3$.

can then be controlled during fabrication, in order to achieve the desired performance. The SC framework is straightforward to implement and, depending on the accuracy required, can be orders of magnitude faster than the traditional MC method. For the examples considered in this paper, we obtain up to two orders of magnitude improvement. This allows one to consider the effect of uncertainties during design and analysis of electrostatic MEMS using high-fidelity computational models.

The proposed methodology is demonstrated by considering two important MEMS devices—switch and resonator. For the MEMS switch example, we study the effect of uncertain material properties and various geometrical features on its actuation behavior. We have shown that, using the information regarding critical design parameters, it is possible to satisfy the desired design criterion without having to prescribe tighter tolerances on all design variables. For the MEMS resonator example, we consider the effect of uncertain parameters on two key quantities of interest—resonant frequency and quality factor. We also analyzed the correspondence between the resonant frequency and the amplitude of the output signal. This illustrates that the explicit representation of the stochastic dependent parameters in terms of the design variables can be used to visualize the solution in stochastic domain, revealing important information regarding device behavior.

APPENDIX
SPARSE GRID INTERPOLATION

Given a smooth function $f : \Gamma \to \mathbb{R}$ and a set of nodes $\Theta_N = \{\boldsymbol{\xi}^i\}_{i=1}^N$, an interpolation can be constructed as follows:

$$f(\boldsymbol{\xi}) \approx \sum_{i=1}^{N} f(\boldsymbol{\xi}^i) L_i(\boldsymbol{\xi}) \tag{A.1}$$

where $f(\boldsymbol{\xi}^i)$ and $L_i(\boldsymbol{\xi}^j) = \delta_{ij}$, $1 \le i, j \le N$, are the function values sampled at the support nodes Θ_N and interpolation basis functions, respectively. Although there exists a well-developed and extensive classical theory of univariate interpolation, such a construction in the multivariate case is not trivial. Much of the research has focused on *selection* of the points $\Theta_N = \{\boldsymbol{\xi}^i\}_{i=1}^N$ such that one achieves a good approximation (to the desired accuracy level). One such possible choice is based on sparse grids generated using the Smolyak algorithm [17], which is considered here. Without loss of generality, we assume that the bounded support of the random variables $\{\xi_i\}_{i=1}^n$ is $\Gamma_i = [0, 1]$, and thus, the bounded random domain $\Gamma = [0, 1]^n$ is an n-hypercube.

Univariate Interpolation

For the 1-D case $(n = 1)$, we assume that $f : [0, 1] \to \mathbb{R}$ is approximated using a sequence of interpolation formulas given as

$$f(\xi) \approx \sum_{i=1}^{m_p} f(\xi^i) \ell(\xi; \xi^i, p) \qquad \forall\, p \ge 1 \tag{A.2}$$

where p refers to the *level of interpolation* and m_p denotes the total number of support nodes, given as

$$m_p = \begin{cases} 1, & \text{if } p = 1 \\ 2^{p-1} + 1, & \text{if } p > 1. \end{cases} \tag{A.3}$$

The support nodes $\{\xi^i\}_{i=1}^{m_p}$ are defined using

$$\{\xi^i\}_{i=1}^{m_p} = \begin{cases} \xi^1 = 0.5 \quad k^1 = 1, & p = 1 \\ \xi^2 = 0.0 \quad \xi^3 = 1.0 \quad k^2 = k^3 = 2, & p = 2 \\ \xi^i = \frac{2(i - m_{p-1}) - 1}{m_p - 1} \quad k^i = p, \quad \text{for } i = m_{p-1}+1, \ldots, m_p; & p \ge 3 \end{cases} \tag{A.4}$$

where ξ^i and k^i denote the *location* and *depth coordinate* for each ith node. We note that the support nodes at any level include the nodes from that level as well as the nodes from all previous levels. For given parameters ξ^i and p, the piecewise linear basis functions are defined using

$$\ell(\xi; \xi^i, p) = 1, \qquad \text{for } p = 1 \tag{A.5}$$

$$\ell(\xi; \xi^i, p) = \begin{cases} 1 - (m_p - 1)|\xi - \xi^i|, & \text{if } |\xi - \xi^i| < \frac{1}{m_p - 1} \\ 0, & \text{otherwise} \end{cases} \tag{A.6}$$

for $p \ge 1$. The 1-D support nodes and corresponding basis functions for various levels of interpolation are shown in Fig. 15. For brevity, we drop the dependence of basis functions on ξ and simply denote $\ell(\xi; \xi^i, p) = \ell(\xi^i, p)$.

Multivariate Interpolation

Tensor Product: Given the univariate interpolation formula, as in (A.2), to obtain an interpolation formula for the

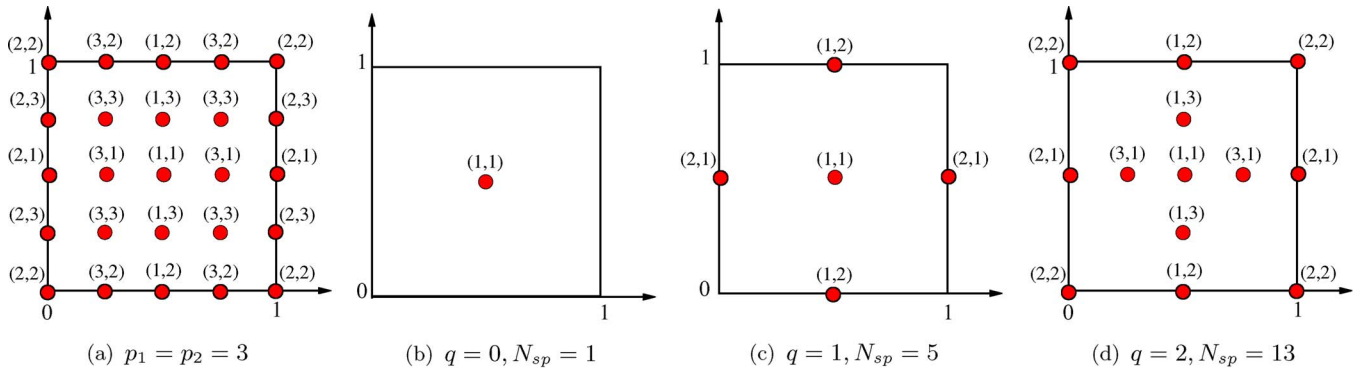

Fig. 16. (a) Tensor and [(b)–(d)] sparse grids for multivariate piecewise linear interpolation. Numbers in parenthesis denote the depth coordinate for each node. (a) $p_1 = p_2 = 3$. (b) $q = 0$, $N_{\rm sp} = 1$. (c) $q = 1$, $N_{\rm sp} = 5$. (d) $q = 2$, $N_{\rm sp} = 13$.

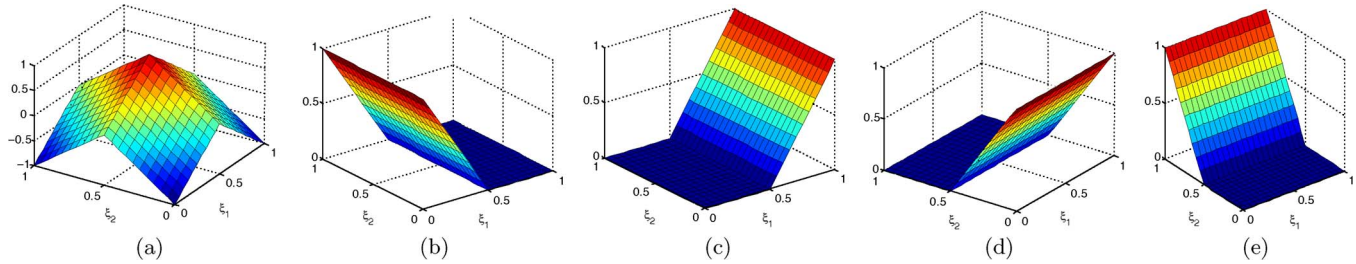

Fig. 17. Interpolation basis functions corresponding to sparse grid for $q = 1$ and $n = 2$. (a) $L_1(\boldsymbol{\xi})$. (b) $L_2(\boldsymbol{\xi})$. (c) $L_3(\boldsymbol{\xi})$. (d) $L_4(\boldsymbol{\xi})$. (e) $L_5(\boldsymbol{\xi})$.

multivariate case, one could simply use tensor product, given as

$$f(\boldsymbol{\xi}) \approx \sum_{i_1=1}^{m_{p_1}} \cdots \sum_{i_n=1}^{m_{p_n}} f(\xi^{i_1}, \ldots, \xi^{i_n}) \cdot \left(\ell(\xi^{i_1}, p_1) \times \cdots \times \ell(\xi^{i_n}, p_n)\right) \quad \text{(A.7)}$$

where $\mathbf{p} = [p_1, \ldots, p_n]$ represents the level of interpolation used in each direction. Clearly, the tensor product formula requires a very high number of support nodes $N = m_{p_1} \cdots m_{p_n}$, which grows rapidly for high dimensions $n \gg 1$. For each ith node $(i = 1, \ldots, N)$, we denote the location and depth coordinate as $\boldsymbol{\xi}^i = (\xi_1^i, \ldots, \xi_n^i)$ and $\mathbf{k}^i = (k_1^i, \ldots, k_n^i)$, respectively.

Smolyak Algorithm: The Smolyak algorithm [17] provides an efficient way to extend the univariate interpolation formula to higher dimensions using the minimal number of support nodes. The algorithm employs tensor products in a special way such that it leads to orders of magnitude reduction in the number of support nodes while maintaining the interpolation quality of the univariate formula for higher dimensions up to a logarithmic factor (see [28] for details). For the case of piecewise linear basis functions, the Smolyak algorithm can be implemented easily using the following.

Selection of Support Nodes:

1) Start with the tensor grid for $p_1 = p_2 = \cdots = p_n = p_0$, where p_0 denotes the level of interpolation in each dimension.
2) Select $0 \leq q \leq p_0 - 1$, denoted as the *sparseness parameter* which governs the accuracy of the approximation. As q increases, we obtain more accurate results.
3) Select all nodes $\boldsymbol{\xi}^i$ with depth coordinate $\mathbf{k}^i$ such that $|\mathbf{k}^i| \leq n + q$, where $|\mathbf{k}^i| = k_1^i + \cdots + k_n^i$, and number them consecutively from $i = 1$ to $N_{\rm sp}$.

For a 2-D problem $(n = 2)$, the tensor grid $(p_1 = p_2 = 3)$ and the corresponding sparse grids for various values of q are shown in Fig. 16.

Construction of Basis Functions: Having selected the support nodes for given q, we construct the basis functions corresponding to ith node $(i = 1, \ldots, N_{\rm sp})$ as follows.

1) We recall that the location and depth coordinate for ith node are given as $\boldsymbol{\xi}^i = (\xi_1^i, \ldots, \xi)$ and $\mathbf{k}^i = (k_1^i, \ldots, k_n^i)$, respectively.
2) From the set of all depth coordinates $\{\mathbf{k}^j\}_{j=1}^{N_{\rm sp}}$, we select those coordinates which satisfy $q + 1 \leq |\mathbf{k}^j| \leq q + n$ and $k_p^j \geq k_p^i, \forall\, p = 1, \ldots, n$. All such *distinct* depth coordinates are added to an index set $\mathcal{K}$ and are numbered consecutively from $j = 1$ to s, such that $\mathcal{K} = \{\mathbf{k}^1, \ldots, \mathbf{k}^s\}$.
3) We construct the basis function for ith node by adding the contributions from all elements in the index set $\mathcal{K}$ as

$$L_i(\boldsymbol{\xi}) = \sum_{j=1}^{s} (-1)^{q+n-|\mathbf{k}^j|} \cdot \binom{n-1}{q+n-|\mathbf{k}^j|} \cdot \ell\left(\xi_1^i, k_1^j\right) \times \cdots \times \ell\left(\xi_n^i, k_n^j\right) \quad \text{(A.8)}$$

where $\binom{a}{b} = a!/(b!(a-b)!)$ denotes the binomial coefficient.

For example, the support nodes [Fig. 16(c)] and basis functions (Fig. 17) for $q = 1$ are given as

$$\begin{aligned} \boldsymbol{\xi}^1 &= (0.5, 0.5) \quad \mathbf{k}^1 = (1,1) \\ L_1(\boldsymbol{\xi}) &= -\ell(0.5,1) \times \ell(0.5,1) \\ &\quad + \ell(0.5,2) \times \ell(0.5,1) \\ &\quad + \ell(0.5,1) \times \ell(0.5,2) \\ \boldsymbol{\xi}^2 &= (0.0, 0.5) \quad \mathbf{k}^2 = (2,1) \end{aligned}$$

$$
\begin{aligned}
L_2(\boldsymbol{\xi}) &= \ell(0.0, 2) \times \ell(0.5, 1) \\
\boldsymbol{\xi}^3 &= (1.0, 0.5) \quad \mathbf{k}^3 = (2, 1) \\
L_3(\boldsymbol{\xi}) &= \ell(1.0, 2) \times \ell(0.5, 1) \\
\boldsymbol{\xi}^4 &= (0.5, 0.0) \quad \mathbf{k}^4 = (1, 2) \\
L_4(\boldsymbol{\xi}) &= \ell(0.5, 1) \times \ell(0.0, 2) \\
\boldsymbol{\xi}^5 &= (0.5, 1.0) \quad \mathbf{k}^5 = (1, 2) \\
L_5(\boldsymbol{\xi}) &= \ell(0.5, 1) \times \ell(1.0, 2).
\end{aligned}
$$

ACKNOWLEDGMENT

The simulations were done using the Turing cluster maintained and operated by the Computational Science and Engineering Program at the University of Illinois.

REFERENCES

[1] S. D. Senturia, N. R. Aluru, and J. White, "Simulating the behavior of MEMS devices: Computational methods and needs," *IEEE Comput. Sci. Eng.*, vol. 4, no. 1, pp. 30–43, Jan. 1997.

[2] G. Li and N. R. Aluru, "Efficient mixed-domain analysis of electrostatic MEMS," *IEEE Trans. Comput.-Aided Design Integr. Circuits Syst.*, vol. 22, no. 9, pp. 1228–1242, Sep. 2003.

[3] S. K. De and N. R. Aluru, "Full-Lagrangian schemes for dynamic analysis of electrostatic MEMS," *J. Microelectromech. Syst.*, vol. 13, no. 5, pp. 737–758, Oct. 2004.

[4] S. K. De and N. R. Aluru, "Coupling of hierarchical fluid models with electrostatic and mechanical models for the dynamic analysis of MEMS," *J. Micromech. Microeng.*, vol. 16, no. 8, pp. 1705–1719, Jul. 2006.

[5] M. Liu, K. Maute, and D. M. Frangopol, "Multi-objective design optimization of electrostatically actuated microbeam resonators with and without parameter uncertainty," *Reliab. Eng. Syst. Saf.*, vol. 92, no. 10, pp. 1333–1343, Oct. 2007.

[6] S. Reh, P. Lethbridge, and D. F. Ostergaard, "Quality based design and design for reliability of micro electro mechanical systems (MEMS) using probabilistic methods," in *Proc. Int. Conf. MSM*, San Diego, CA, 2000, pp. 708–711.

[7] J. S. Kong, D. M. Frangopol, M. Rauli, K. Maute, R. A. Saravanan, L. A. View, and R. Raj, "A methodology for analyzing the variability in the performance of a MEMS actuator made from a novel ceramic," *Sens. Actuators A, Phys.*, vol. 116, no. 2, pp. 336–344, Oct. 2004.

[8] M. Allen, M. Rauli, K. Maute, and D. Frangopol, "Reliability-based analysis and design optimization of electrostatically actuated MEMS," *Comput. Struct.*, vol. 82, no. 13/14, pp. 1007–1020, May 2004.

[9] J. S. Han and B. M. Kwak, "Robust optimal design of a vibratory microgyroscope considering fabrication errors," *J. Micromech. Microeng.*, vol. 11, no. 6, pp. 662–671, Oct. 2001.

[10] R. Liu, B. Paden, and K. Turner, "MEMS resonators that are robust to process-induced feature width variations," *J. Microelectromech. Syst.*, vol. 11, no. 5, pp. 505–551, Oct. 2002.

[11] J. Wittwer, M. S. Baker, and L. L. Howell, "Robust design and model validation of nonlinear compliant micromechanisms," *J. Microelectromech. Syst.*, vol. 15, no. 1, pp. 33–41, Feb. 2006.

[12] N. Agarwal and N. R. Aluru, "A stochastic Lagrangian approach for geometrical uncertainties in electrostatics," *J. Comput. Phys.*, vol. 226, no. 1, pp. 156–179, Sep. 2007.

[13] N. Agarwal and N. R. Aluru, "Stochastic modeling of coupled electromechanical interaction for uncertainty quantification in electrostatically actuated MEMS," *Comput. Methods Appl. Mech. Eng.*, vol. 197, no. 43/44, pp. 3456–3471, Aug. 2008.

[14] D. Xiu and J. S. Hesthaven, "High-order collocation methods for differential equations with random inputs," *SIAM J. Sci. Comput.*, vol. 27, no. 3, pp. 1118–1139, 2005.

[15] B. Ganapathysubramanian and N. Zabaras, "Sparse grid collocation schemes for stochastic natural convection problems," *J. Comput. Phys.*, vol. 225, no. 1, pp. 652–685, Jul. 2007.

[16] I. Babuska, F. Nobile, and R. Tempone, "A stochastic collocation method for elliptic partial differential equations with random input data," *SIAM J. Numer. Anal.*, vol. 45, no. 3, pp. 1005–1034, May 2007.

[17] S. Smolyak, "Quadrature and interpolation formulas for tensor products of certain classes of functions," *Sov. Math. Dokl.*, vol. 4, pp. 240–243, 1963.

[18] D. S. Chandrasekharaiah and L. Debnath, *Continuum Mechanics*. New York: Academic, 1994.

[19] G. Li and N. R. Aluru, "A Lagrangian approach for electrostatic analysis of deformable conductors," *J. Microelectromech. Syst.*, vol. 11, no. 3, pp. 245–254, Jun. 2002.

[20] E. S. Hung and S. D. Senturia, "Generating efficient dynamical models for microelectromechanical systems from a few finite-element simulation runs," *J. Microelectromech. Syst.*, vol. 8, no. 3, pp. 280–289, Sep. 1999.

[21] N. R. Aluru and J. White, "An efficient numerical technique for electromechanical simulation of complicated microelectromechanical structures," *Sens. Actuators A, Phys.*, vol. 58, no. 1, pp. 1–11, Jan. 1997.

[22] D. Xiu and G. E. Karniadakis, "The Wiener-Askey polynomial chaos for stochastic differential equations," *SIAM J. Sci. Comput.*, vol. 24, no. 2, pp. 619–644, 2002.

[23] M. D. McKay, R. J. Beckman, and W. J. Conover, "A comparison of three methods for selecting values of input variables in the analysis of output from a computer code," *Technometrics*, vol. 2, no. 1, pp. 239–245, Feb. 1979.

[24] H. Niederreiter, *Random Number Generation and Quasi-Monte*. Philadelphia, PA: SIAM, 1992.

[25] W. Gilks, S. Richardson, and D. Spiergelhalter, *Markov Chain*. London, U.K.: Chapman & Hall, 1995.

[26] G. Lin, C. H. Su, and G. E. Karniadakis, "Random roughness enhances lift in supersonic flow," *Phys. Rev. Lett.*, vol. 99, no. 10, p. 104 501, Sep. 2007.

[27] B. McCarthy, G. G. Adams, N. E. McGruer, and D. Potter, "A dynamic model, including contact bounce, of an electrostatically actuated microswitch," *J. Microelectromech. Syst.*, vol. 11, no. 3, pp. 276–282, Jun. 2002.

[28] V. Barthelmann, E. Novak, and K. Ritter, "High dimensional polynomial interpolation on sparse grid," *Adv. Comput. Math.*, vol. 12, no. 4, pp. 273–288, Mar. 1999.

Nitin Agarwal received the B.Tech. degree in mechanical engineering from the Indian Institute of Technology, Bombay, India, in 2002 and the M.S. and Ph.D. degrees from the University of Illinois at Urbana–Champaign (UIUC), Urbana, in 2005 and 2009, respectively.

During his doctoral research at UIUC, he received the Computational Science and Engineering fellowship during 2006–2007 and the Beckman Institute Graduate Student fellowship during 2008–2009. His research interests are scientific computing, stochastic multiphysics simulations, uncertainty quantification, and computational microelectromechanical systems.

Narayana R. Aluru received the B.E. degree (with honors and distinction) from the Birla Institute of Technology and Science (BITS), Pilani, India, in 1989, the M.S. degree from Rensselaer Polytechnic Institute, Troy, NY, in 1991, and the Ph.D. degree from Stanford University, Stanford, CA, in 1995.

From 1995 to 1997, he was a Postdoctoral Associate at the Massachusetts Institute of Technology (MIT), Cambridge. In 1998, he joined the University of Illinois at Urbana–Champaign (UIUC), Urbana, as an Assistant Professor. He is currently the Richard W. Kritzer Distinguished Professor in the Department of Mechanical Science and Engineering, UIUC. He is also affiliated with the Beckman Institute for Advanced Science and Technology, the Department of Electrical and Computer Engineering, and the Bioengineering Department, UIUC.

Dr. Aluru is a Subject Editor for the JOURNAL OF MICROELECTROMECHANICAL SYSTEMS and currently serves on the Editorial Board of a number of other journals. He served as the Associate Editor for the IEEE TRANSACTIONS ON CIRCUITS AND SYSTEMS II during 2004–2005. He was the recipient of the NSF CAREER Award in 1999, the NCSA faculty fellowship in 1999 and 2006, the 2001 CMES Distinguished Young Author Award, the Xerox Award for Faculty Research in 2002, the ASME Gustus L. Larson Memorial Award in 2006, and the USACM Gallagher Young Investigator Award in 2007, and was named a Willett Faculty Scholar by the College of Engineering, UIUC, for the period 2002–2008.